Monte Carlo Simulations of the Morphology of ABC Star Polymers Using the Diagonal Bond Method

Tohru Gemma,*,† Akira Hatano,‡ and Tomonari Dotera§

Department of Basic Science, University of Tokyo, Komaba, Meguro-ku, Tokyo 153-8902, Japan; Department of Information System, Teikyo Heisei University, Uruido, Ichikawa, 290-0193, Japan; and Saitama Study Center, The University of the Air, 682-2 Nishiki-cho, Saitama 331-0851, Japan

Received June 15, 2000; Revised Manuscript Received August 31, 2001

ABSTRACT: The microphase-separated morphology of ABC three-arm star-shaped copolymers with arm-length ratio 1:1:*x* is investigated by a recently proposed simulation method, the diagonal bond method. Five kinds of two-dimensional (cylindrical) phases, three kinds of lamellar-type phases and two kinds of continuous matrix phases are discovered. The phase diagram is presented: The progression of the morphologies as a function of *x* is the following: lamella + sphere; five polygonal cylinders, [8.8.4], [6.6.6], [8.6.4; 8.6.6], [10.6.4; 10.6.4; 10.6.6], [12.6.4]; perforated layer; lamella + cylinder; columnar piled disk; lamella-in-sphere. Two remarkable features of ABC star polymer systems are found: first, in all phases junction point monomers gather on lines where three interfaces meet, and second, the section of the cylindrical phase becomes the tessellation of even-numbered polygons. The free energy of the system is also calculated in the strong segregation limit for four kinds of simple phases, and the results are consistent with the simulations.

I. Introduction

Microphase-separated structures of block copolymers have received much attention over many years.[1−15] A wide variety of morphologies with changing block copolymer composition has been studied extensively both in theoretical and experimental points of view. In contrast to substantial studies on AB diblock and linear ABC triblock copolymers, there is no clear understanding of the morphology of branched copolymers, mainly because there are experimental difficulties, e.g., in the selection of polymer−polymer and polymer−solvent combinations, in synthesizing well-characterized branched copolymers, and in structure determination as well. However, star-shaped[16] or comb-shaped[17,18] copolymer systems are considered to be very fascinating because one expects to find novel morphologies.

Recently, ABC three-arm star-shaped copolymers, referred to as "ABC star polymer", (Figure 1a) were synthesized by several groups.[19−27] Independently, our numerical experiment revealed a three-colored honeycomb structure in the case of ABC star polymer with equal arm lengths, provided interaction parameters between three components are equal strength.[10] This numerical result seems to be correct, however, Sioula et al. found a different structure in star−(polystyrene; polyisoprene; poly(methyl methacrylate)) of which the volume fraction ratio was 1.3:1:1.2.[27] The experimental structure may be the consequence of large asymmetry in interaction parameters as described in their report, or solvents might have affected the structure formation of microdomains.

Like the above-mentioned case, one can hardly avoid complicated situations in experimental systems. However, on the first step, numerical methods under simple and well-defined conditions will contribute to the general understanding of fundamental phase behavior of ABC star systems, aiming to be guides for experimental plans, and to evoke theoreticians' ideas as well. Then, on the next step, we are able to proceed to more specific conditioned simulations, which are expected to predict detailed phase behavior or reproduce experimental results. The objective of the paper is to put the first step forward for ABC star systems with AB symmetry. We would like to uncover various morphologies in the ABC star polymer melts even by changing the fraction of the C component.

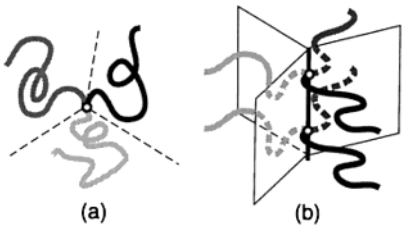

Figure 1. (a) ABC star polymer consisting of a junction point monomer and three arms of different chemical species A, B, and C. Between the three arms, three interfaces appear. (b) Junction point line (JPL). Junction point monomers depicted by small circles must gather on a line where three interfaces meet.

In the previous work,[10] we proposed the *diagonal bond method* (DBM), a new Monte Carlo simulation method for block copolymer systems, and with the implementation of efficient C codes, outstanding performance at that time was demonstrated. It is because the DBM is a lattice polymer simulation method that allows polymer bonds to lie along both face and body diagonal directions on a cubic lattice in addition to edges. An important bonus of using diagonal bonds is to increase not only possible conformations of the lattice polymers but also vast moving ways of monomers and bonds. Furthermore, by allowing bond crossings and phantom-chain moves, remarkable acceleration of chain motion and microphase-separation ordering are achieved. The DBM is also very suited for branched polymer systems, because it enables branching-monomer motion

* Corresponding author.
† University of Tokyo.
‡ Teikyo Heisei University.
§ The University of the Air.

10.1021/ma001040q CCC: $22.00
Published on Web 02/22/2002

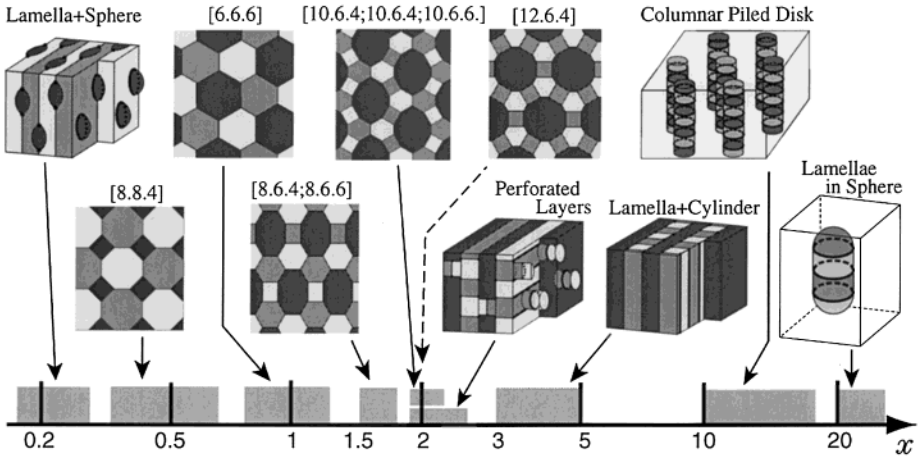

Figure 2. Phase diagram of ABC star polymer systems with arm-length ratio 1:1:*x* and with symmetric interactions between three components. A (light gray), B (medium gray), and C (dark gray) are displayed. Junction point lines are drawn by thick lines or solid circles where three kinds of interfaces meet. Morphologies are lamella + sphere (L + S), five cylindrical structures in sectional view denoted by polygons around a vertex in the sections ([8.8.4], [6.6.6], [8.6.4; 8.6.6], [10.6.4; 10.6.4; 10.6.6], [12.6.4]), perforated layer (PL), lamella + cylinder (L + C), columnar piled disk (CPD), and lamella-in-sphere (L-in-S). Notice that the [12.6.4] phase does not possess A−B permutation symmetry.

by using diagonal bonds; it has been successfully applied to ABC star polymers, and also to ABCD star polymers, leading to the discovery of a new morphology called "cell crystals".[12]

Molecular architecture affects morphologies. The case of ABC star polymers provides a striking example of this statement, because it is crucially different from the case of linear block copolymers or AB_2-type star polymers[28] in the state of junction points; in the former, they are concentrated on lines rather than scattered at the interfaces of microdomains. As depicted in Figure 1b, three arms of star polymers segregate each other, and consequently, junction points assemble a line where three interfaces meet, provided interaction parameters between three components are strong enough. Hereafter, we will call this line a *junction point line* (JPL). JPLs may take various geometrical shape, e.g., straight lines, circles, wavy lines, and so on. However, there are no end-points of JPLs; they should become closed lines or go off the surfaces of materials. The existence of JPLs becomes a strong topological constraint as we will later see.

Before going into details, we would like to summarize the results of our simulations by displaying Figure 2: a schematic phase diagram of the ABC star polymers with arm-length ratio $N_A:N_B:N_C = 1:1:x$. There are several remarkable features in the phase diagram.

1. Every domain (A, B, or C) contacts all other polymer components. This is the consequence of the existence of JPLs drawn by thick lines or solid circles. JPLs are circles or parallel straight lines schematically.

2. In extensive midrange, there are five cylindrical phases having polygonal cross-sections illustrated in a sectional view. A set of integers [*k.l.m*] is assigned to the cylindrical phases, representing that *k*-gon, *l*-gon, and *m*-gon appear in the cross-sections. More precise definitions will be given later.

3. All polygons are even-numbered: tetragons, hexagons, octagons, decagons, and dodecagons. This is a strong geometric constraint in this system so that we will state it as a theorem; a similar theorem holds for the ABCD star polymer system.[12]

4. A class of cylindrical phases composed of only one type of JPLs exists. There are three and only three types in this class.

5. Viewing the development of the cylindrical phases as a function of *x*, the number of vertices of C polygons increases as 4, 6, 8, 10, and/or 12. Finally, the vertex number reaches infinity (L + C).

6. As another aspect of the section of the cylindrical phases, except for [8.8.4], the arrangement of C islands is hexagonal in the sea of A and B. This hexagonal arrangement is in common with other copolymer systems.

7. The obtained morphologies in order of *x* are lamella + sphere (L + S),[29] [8.8.4], [6.6.6], [8.6.4; 8.6.6], [10.6.4; 10.6.4; 10.6.6], [12.6.4], perforated layer (PL), lamella + cylinder (L + C),[13] columnar piled disk (CPD), and lamella-in-sphere (L-in-S) phases.[17]

8. In a small *x* region, the structural change of the C component from spheres (L + S) to cylinders (five cylindrical phases) and from cylinders to layers (L + C) can be understood to be analogous to that of AB-diblock copolymers.

9. In a large *x* region, the structural change of A and B components from layers (L + C) to cylinders (CPD) and from cylinders (CPD) to spheres (L-in-S) can be explained in analogy with that of AB-diblock copolymers. This progression containing hierarchical structures has been recognized for comb polymers.[17]

10. Three phases has been observed around $x = 2$, for which we cannot decide a stable phase. On the contrary, almost all attempts failed to obtain ordered structures at $5 < x < 10$. We think that large scale simulations of star polymers having longer chain lengths can resolve them.

The remainder of this paper is organized as follows. The simulation method DBM is briefly given in the next section and the details of the above-mentioned phases are described in section III. Section IV is devoted to consideration on geometric properties of the cylindrical phases, characteristic of ABC star polymer systems: The *even-polygon theorem* is presented, and the notion of the *single JPL class* and the *plural JPL class* is introduced. We clarify how many types belong to the single JPL class. In section V, we calculate the free energy of some structures in the strong segregation limit, which turns out to be consistent with Figure 2. In the last section, a conclusion is given. In Appendix A, detailed calculations of the free energy are given, and

in Appendix B, an interface bend effect on the cylindrical phase [8.8.4] is discussed as an example. Since the existence of JPLs is a remarkable feature of ABC star polymer systems, we will always pay our attention to JPLs in this paper, as well as to microphase-separated domain structures.

II. Simulation Method

Details of Monte Carlo simulations with the DBM have been reported in a previous paper;[10] hence, we here describe only a brief outline.

One ABC star polymer consists of N_A A-type beads, N_B B-type beads, N_C C-type beads, and one Y-type bead (junction point monomer), which are connected by $N - 1$ bonds, where $N = N_A + N_B + N_C + 1$. In the real polymer system, there may be cases where a synthesized ABC star polymer does not contain a different monomer such as the Y-type bead at the junction point. However, the junction-point monomer is necessary for the simulation of branched polymers on the lattice. If we replace the Y-type with one of A, B or C-type monomer, then the symmetry for A, B, and C cannot be retained. Therefore we employ a Y-type monomer.

Beads are placed on the simple cubic lattice, and bonds are allowed not only along the edges of the cubic lattice but also along face diagonals and body diagonals. The excluded volume effect is dealt with only for beads in that two or more beads cannot occupy one lattice point at the same time, while two or three bonds can cross each other. This treatment has been verified.[10]

Energy of the system is the summation of contact energies $\epsilon_{\alpha\beta}$; when α and β beads are within $\sqrt{3}$ lattice spacing, $\epsilon_{\alpha\beta}$ is given. Since in the DBM face and body diagonals are within the interaction-range, there are 26 sites around one site. In this study, we assume symmetric interactions

$$\epsilon_{AB} = \epsilon_{BC} = \epsilon_{CA} = \epsilon_{AY} = \epsilon_{BY} = \epsilon_{CY} = 1$$

otherwise

$$\epsilon_{\alpha\alpha} = 0$$

Whole simulation systems are mainly cubic boxes of size L^3 with $L = 16-50$, on which periodic boundary conditions of x, y, and z directions are imposed. Twenty-five percent of lattice sites are left vacant in order that beads can move. The vacant sites act as nonselective solvents. A bead move is ruled by the Metropolis algorithm. The elementary move is as follows: first, one bead in the system and one of its movable sites are selected randomly; second, if the site is vacant, the energy after the move is calculated, otherwise, go back to the first step; third, if δE is negative or zero, the bead move is accepted, otherwise the probability of the bead move is $e^{-\beta\delta E}$, where β is the inverse temperature.

Monte Carlo calculations are carried out according to the following procedure:

1. Place ABC star polymers regularly.
2. Randomize the polymer arrangement by running at the infinite temperature ($\beta = 0$).
3. Quench the system at a finite temperature and wait for structure ordering.

Quenching was usually performed at $\beta \simeq 0.1$, unless otherwise noted. When $x \leq 1/3$ or $x \geq 5$, the quenching has been made in two steps: first at a high temperature where longer chains order and second at a low temperature where shorter chains order. We restrict our investigation to final morphologies.

The acceptance ratio is defined as the rate of acceptance of trial moves per one random selection of a monomer. Figure 3 shows the energy per monomer and the acceptance ratio plotted vs Monte Carlo steps for a system consisting of 9-9-9 star polymers. The ratio and energy are calculated at every one hundred Monte Carlo steps. The plotted acceptance ratio and energy are averaged values over each 10 000 Monte Carlo steps. In practice, they were averaged over 100 samples measured at each 100 MC steps.

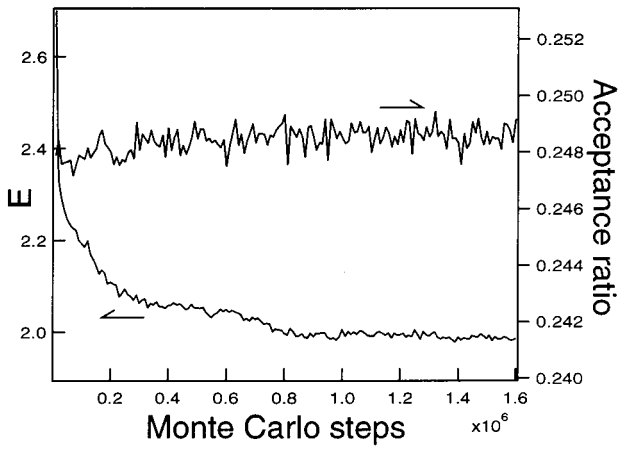

Figure 3. Acceptance ratio and energy per monomer vs Monte Carlo step are shown for a system with (N_A, N_B, N_C) = (9, 9, 9) in a $L = 30$ box at $\beta = 0.1$. The acceptance ratio almost always takes a value near 0.248. As for the energy, the plot shows an initial rapid decrease and a successive quasistationary period. There exists a slight drop around 0.8 million steps, which corresponds to the formation of the ordered [6.6.6] phase.

As shown in Figure 3, the ratio is almost the ratio of vacant sites to the total lattice sites in the full simulation history. In other words, the ratio is restricted only by the excluded volume effect, which is inevitable for all lattice type simulations. It means the highest effectiveness, which is one of the merits of the DBM.[10]

The judgment on the formation of an ordered structure was done in two ways together: visual observations of domain shapes on a computer terminal and observations of energy changes of the system. Two observations coincide, for example, as shown in Figure 3, where the visual observation of structure ordering of the [6.6.6] cylindrical phase exactly corresponds to an energy drop at about 0.8 million MC steps.

A Monte Carlo sweep to reach an ordered structure took typically several hundred thousands MC steps in the case of comparatively small systems, such as $L \leq 30$. In the case of $L \geq 40$, it often reached several tens of millions. After a fair amount of computation, if the domain shape is ill-ordered and if it appears not to change any more, then we judge the run is trapped in a quasi-stable state. We restart quenching with different initial conditions. Even if an ordered structure appears, we have performed multiple attempts to enhance its reliability.

It should be mentioned that the segregation power was fairly strong and thus simulations were performed in the strongly segregated regime. To estimate χ, we use the following expression for the lattice model

$$\chi_{\alpha\beta} = (z - 2)\,\beta\left[\epsilon_{\alpha\beta} - \frac{(\epsilon_{\alpha\alpha} + \epsilon_{\beta\beta})}{2}\right] \qquad (1)$$

where $\chi_{\alpha\beta}$ is the interaction parameter between α and β monomers and z is the number of the nearest neighboring sites. In our simulation model, $z = 26$. Taking account of the monomer density on the lattice 0.75, we employed 0.75×24 for the value of $z - 2$. Because of the symmetric interactions; $\epsilon_{\alpha\beta} = 1$ ($\alpha \neq \beta$) and $\epsilon_{\alpha\alpha} = 0$, three interaction parameters between three components have the same value: $\chi = \chi_{AB} = \chi_{BC} = \chi_{CA} = 18\,\beta$.

Consequently, we have only one parameter $N\chi$ which represents the segregation power of the system. In the typical case of the present simulations, $N \simeq 30$ and $\beta \simeq 0.1$, that is, $N\chi \simeq 54$, and even in the smallest case, $N\chi$ is 45.

III. Results of Monte Carlo Simulation

In this section, we describe results in order of arm-length ratio x. We also provide some definitions, expla-

Table 1. Simulation Results for Star Polymers with Arm Length Ratio 1:1:*x* under Symmetric Interactions[a]

x	N_A	N_C	L	morphology
0.17	30	5	36	L + S
0.25	16	4	38	L + S
0.31	16	5	40	L + S
0.33	30	10	33	L + S
0.37	30	11	34	[8.8.4]
0.38	16	6	36, 38	[8.8.4]
0.4	30	12	32	[8.8.4]
0.5	10	5	33, 40	[8.8.4]
	16	8	51	[8.8.4]
	20	10	40	[8.8.4]
	40	20	42	[8.8.4]
0.7	10	7	34	[8.8.4]
0.8	10	8	26	[6.6.6]
0.9	10	9	32	[6.6.6]
1.0	9	9	40, 60	[6.6.6]
	10	10	25, 28	[6.6.6]
	14	14	33, 37, 40	[6.6.6]
	20	20	37, 38, 40	[6.6.6]
	28	28	41	[6.6.6]
1.1	10	11	28	[6.6.6]
1.2	10	12	29	[6.6.6]
	20	24	40	[6.6.6]
1.5	8	12	32	[8.6.4]
1.75	8	14	31	[8.6.4]
1.875	8	15	29, 30, 31	[10.6.4]
	8	15	30	PL
2.0	8	16	29−31[b]	[10.6.4]
	8	16	21, 25, 27, 29	PL
	9	18	32	[10.6.4]
	8	16	25, 26	[12.6.4]
2.125	8	17	31, 32	[10.6.4]
	8	17	30, 34	PL
2.25	8	18	32	[10.6.4]
	8	18	24−42	PL
2.5	8	20	31, 35	PL
3.0	8	24	30, 32, 33, 36	L + C
5.0	5	25	32	L + C
8.0	5	40	35	IPL
10	5	50	38	CPD
12	5	60	40	CPD
15	4	75	24	CPD
18	5	90	45	CPD
20	4	80	26,32	L-in-S
	10	200	50	L-in-S
25	5	125	30,37	L-in-S
	8	200	50	L-in-S

[a] N_α is the length of an α arm and L is the size of a simulation cube. Morphologies are explained in the main text. [b] $22^2 \times 28$, $22^2 \times 30$, $30^2 \times 32$, $(29 \sim 31)^2 \times 33$, $66 \times 60 \times 10$.

nations and implications. Conditions and results of the simulations are summarized in Table 1.

A. 0.17 ≤ *x* ≤ 0.33: Lamella + Sphere. The obtained structure is shown in Figure 4. The shorter chain component C makes oblate spherical domains, while the longer chain components A and B form alternating lamellar layers. The C spheres exist on the AB interfaces and seem to be arranged hexagonally. We refer to this structure as lamella + sphere (L + S).[29] The snapshot in Figure 4 has been obtained in the (N_A, N_B, N_C) = (16, 16, 4) system in a $L = 38$ box. In this case, L + S phase has formed at $\beta \geq 0.15$ ($N\chi \geq 100$). In the temperature range $0.05 < \beta < 0.15$, A and B arms have formed the lamellae, while C arms uniformly spread in A−B interface regions and have not yet been ordered.

In this phase, the junction point monomers are at the AB interface with surrounding the C domains; thus, the JPLs are circles as depicted by thick lines in Figure 4. From the knowledge of diblock copolymer systems, alternating lamellae of the two major components is a plausible structure when x is close to 0.

In our small-size simulations, AB lamellae have formed perpendicular to both [100] and [111] of the simulation box. We have seen that intrainterface C-domain ordering seems hexagonal. We note that because of the quenching process the fluctuation of C-domain volumes has been still large (Figure 4b), hindering satisfactory ordering. Moreover, one may think stacking order of the hexagonal layers, however, we have not clarified interinterface C domain ordering, partly because the restriction imposed by periodic boundary conditions (e.g. [111]) is stronger than the strength of the interinterface ordering.

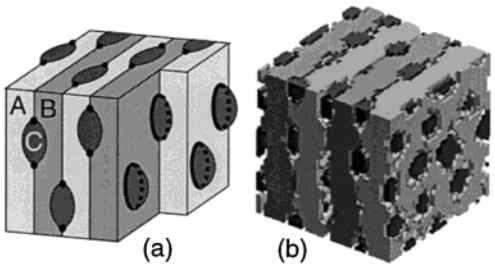

Figure 4. (a) Schematic illustration of the lamella + sphere (L + S) phase. When $x \leq 0.33$, A and B components make alternating layers and C domain forms oblate spheres at interfaces. The JPL (thick lines) is a circle surrounding a C sphere. (b) Snapshot of the simulation of (N_A, N_B, N_C) = (16, 16, 4) in a $L = 38$ box. A is light gray, B is medium gray, and C is dark gray. The snapshot displays a very low temperature structure to see the domain boundaries vividly ($\beta \simeq 2$). The following pictures (Figure 5, parts 7−14) render very low-temperature structures for the same reason.

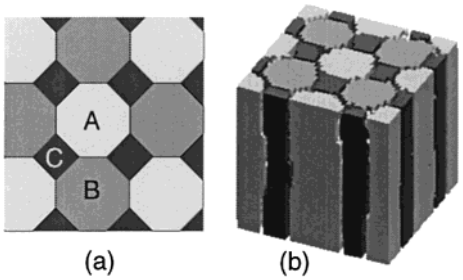

Figure 5. (a) Schematic cross-section of the [8.8.4] cylindrical phase found at $x = 0.38-0.7$. The interfaces are simplified by straight lines. (b) Snapshot of a simulated structure for (N_A, N_B, N_C)=(20,20,10) in a $L = 40$ system. A is light gray, B is medium gray, and C is dark gray.

B. 0.37 ≤ *x* ≤ 0.7: [8.8.4] Cylinder. In this region, a cylindrical structure with square symmetry (D_{4h}) as shown in Figure 5 has been obtained. Longer chain components A and B revealed octagonal sections, while shorter C chains formed square sections. The number density of C domains is found twice of A and B domains. Boundaries between domains of A and B appeared to be flat; it agrees with the symmetry requirement for A and B components. However, CA and BC interfaces are not necessarily flat. In a system with relatively long chains, (N_A, N_B, N_C) = (40, 40, 20), boundaries of C domains appeared to be slightly convex outward. This makes the reduction of the interface area as discussed in Appendix B.

To classify cylindrical structures, we employ the terminology of tiling problems.[30] We assign a polygonal tiling pattern a set of numbers [$k_1k_2...k_l$] which indicates that a vertex in the tiling is surrounded by k_1-gon, k_2-gon, ..., and k_l-gon. Since, in the cross-section of a cylindrical phase, a vertex is the projection of a JPL, l must equal three in our problem. Thus we put three numbers as [$k_1.l_1.m_1$] denoting a cylindrical structure. If there are two types of vertices in a section,

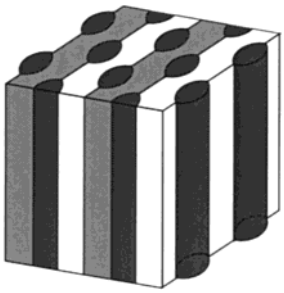

Figure 6. Lamella + rod (L + R) structure. When C arms become longer than the L + S phase, spherical domains grow within interfaces between A and B, and at last may connect each other; then the C component may form rods at the interfaces. The rod corresponds to a cylinder of vertex number = 2. However, this structure has not been obtained in the present work.

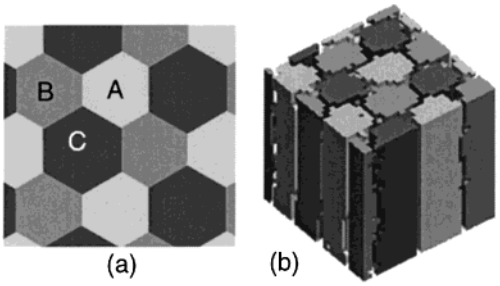

Figure 7. (a) Schematic cross-section of the [6.6.6] cylindrical phase found at $x = 0.8-1.2$. This sectional view is drawn for the case $x > 1$. (b) Snapshot of a simulated structure of (N_A, N_B, N_C) = (12, 12, 12) with $L = 32$. A is light gray, B is medium gray, and C is dark gray.

it is designated by two sets of three numbers [$k_1.l_1.m_1;k_2.l_2.m_2$]. For the present structure with square symmetry, we refer to it as [8.8.4].

Between L + S and [8.8.4], we have searched for the lamella + rod phase (L + R)[29] shown in Figure 6, but have not found it. In some runs for (N_A, N_B, N_C) = (16,-16,6), AB lamellae have been formed at a rather high temperature, $\beta \simeq 0.07$ ($N\chi = 49$), while the C component has no order at AB interfaces. This structure, however, has changed to the [8.8.4] cylinder upon lowering temperature to $\beta \geq 0.115$ ($N\chi \geq 81$). For the meantime, we conclude that the L + R phase does not appear in ABC star polymer system with $N_A = N_B$ and symmetric interactions.

The above-mentioned structure transformation upon lowering temperature is an unique example of stepwise transformations observed in the whole present simulations. Stepwise transformations are expected to occur in complex systems consisting of more than three components. The problem of order−order structure transformations by changing $N\chi$ will be a subject for future investigations.

C. 0.8 ≤ *x* ≤ 1.2: [6.6.6] Cylinder. It has been already reported that the three-colored honeycomb structure was found for ABC star polymers with all three arms of the same length.[10] As shown in Figure 7, this structure is designated as [6.6.6]. In this work, it is confirmed that [6.6.6] is formed in the range of $0.8 \leq x \leq 1.2$. For $x = 1.0$, we have also confirmed the formation of [6.6.6] up to $L = 60$. The case where N_C is slightly larger than $N_A = N_B$ is depicted in Figure 7a.

D. 1.5 ≤ *x* ≤ 1.75: [8.6.4; 8.6.6] Cylinder. Figure 8a shows the schematic section of a cylindrical structure, which has been found for (N_A, N_B, N_C) = (8, 8, 12) and

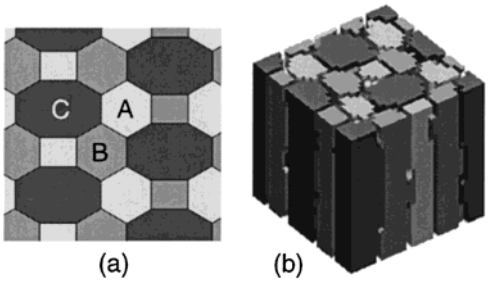

Figure 8. (a) Schematic cross-section of the [8.6.4; 8.6.6] cylindrical phase found at $x = 1.5-1.75$. For simplicity, all edges are drawn straight. (b) Snapshot of a simulated structure of (N_A, N_B, N_C) = (8, 8, 14) in a $L = 31$ box. A is light gray, B is medium gray, and C is dark gray.

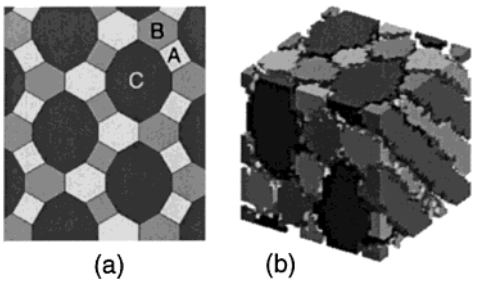

Figure 9. (a) Schematic cross-section of the [10.6.4; 10.6.4; 10.6.6] cylindrical phase found at $1.875 \leq x \leq 2.25$. For simplicity, all edges are drawn straight. (b) Snapshot of a simulated structure of (N_A, N_B, N_C) = (8, 8, 16) with $L = 31$. A is light gray, B is medium gray, and C is dark gray.

(8, 8, 14). There are two types of vertices (JPLs), [8.6.4] and [8.6.6]; this is then called [8.6.4; 8.6.6] (hereafter abbreviated as [8.6.4]). An octagonal C-domain is surrounded alternately by A and B domains consisting of six hexagons and two tetragons. We have found the [8.6.4] phase only in the simulation boxes of $L = 31$ and $L = 32$. To confirm that the phase is a stable phase, large scale simulations are needed.

E. *x* ≈ 2. In the present simulation study, we have not been able to determine a unique morphology near $x = 2$, because three kinds of morphologies have appeared as results of many simulation runs for the star polymers of (N_A, N_B, N_C) = (8,8,15), (8,8,16), (8,8,17) and (8,8,-18).

E1. [10.6.4; 10.6.4; 10.6.6] Cylinder. One is a cylindrical structure [10.6.4; 10.6.4; 10.6.6] (hereafter abbreviated as [10.6.4]), which has been found in the range $1.875 \leq x \leq 2.25$. Figure 9 shows the schematic illustration of a section. The longer chain C component makes decagonal domains, surrounded by six hexagons and four tetragons. There exist three kinds of JPLs: one [10.6.6] type and two [10.6.4] types.

In the case of cubic boxes, the [10.6.4] phase has been found only near $L = 31$ for (8,8,16). Varying the size Lx while keeping $L_x = L_y$, we have found that the lattice constants are about $22^2 \times 30$. Therefore, the phase is formed in the (1,1,0) direction in the cube of $L = 31$. Although we have failed to form the phase in larger simulation boxes, at least in a quasi-two-dimensional box of sizes $60 \times 66 \times 10$, this phase has been easily obtained.

For the cylindrical phase series, the vertex number of polygons composed of C arms becomes larger, $4 \rightarrow 6 \rightarrow 8$ with increasing x; the appearance of the decagonal C-cylinder is in due course. It would be interesting that along this sequence, the C monomers make dodecagons

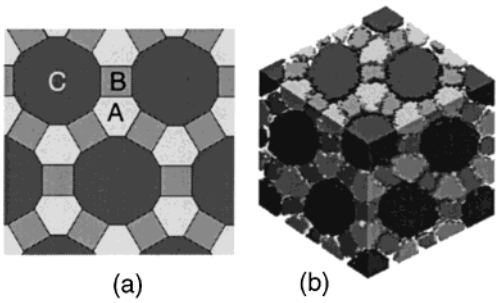

Figure 10. (a) Schematic cross-section of the [12.6.4] cylindrical phase found at $x \sim 2$, $N_A > N_B$. (b) Snapshot of a simulated structure of $(N_A, N_B, N_C) = (8, 6, 16)$ in a $L = 42$ box. A is light gray, B is medium gray, and C is dark gray. The cylinders lie along the [111] direction of the cube.

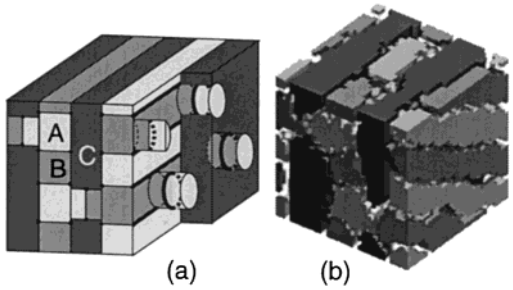

Figure 11. (a) Schematic illustration of the perforated layer (PL) phase at $1.875 \le x \le 2.5$. C arms make perforated layers and A and B form rectangular cylinders alternately arranged between C layers. There are two types of JPLs: one type is a circular line in the hole of the C layer and another is drawn as a straight line along the cylinder of A and B components. (b) Snapshot of a simulated structure of $(N_A, N_B, N_C) = (8, 8, 16)$ with $L = 29$. A is light gray, B is medium gray, and C is dark gray.

with keeping AB permutation symmetry. For the case of (8,8,18), there has been no indication of such a formation even in quasi-two-dimensional simulations. It appears that the composition $x = 2.25$ is the outside of the cylindrical phase region.

E2. [12.6.4] Cylinder. As shown in Figure 10, there are C polygons with the largest vertex-number 12 in the present paper. The dodecagonal domain of C is alternately surrounded by six hexagons and six tetragons, which are occupied by the shorter components, A and B. Unlike [8.6.4] or [10.6.4], all hexagons are occupied by one of two components and all tetragons are occupied by the other component. Therefore, the permutation symmetry of AB is broken in this phase.

On one hand, we do not deny the observation is due to the small size simulation, whose boundary conditions force the system strongly to form a quasistable structure. On the other hand, the structure is feasible under asymmetric conditions as is expected in realistic cases. In fact, we have found this phase easily when $N_A \neq N_B$, for example, in the cases of $(N_A, N_B, N_C) = (8, 6, 16)$, $L = 25$, 31 and 42 (Figure 10b). Recently, Takano et al.[26] synthesized star polymers (poly(α-methylstyrene); polyisoprene; poly(2-vinylpyridine)). In the TEM picture of their ABC star polymer with 0.25:0.25:0.5 composition, they found a similar structure to Figure 10.

E3. Perforated Layer. Another structure we have found is a perforated layer (PL) structure (Figure 11). Perforated layers are formed by a longer chain component C, while A and B components alternately make rectangular cylindrical domains between C-layers. Into the holes of a C-layer, A and B domains enter from both sides. This structure has been found in the range $1.875 \le x \le 2.5$. There are two types of JPLs: circles in the holes of C-layers and straight lines along the rectangular cylinders. This is another type of the broken symmetry of the state of JPLs.

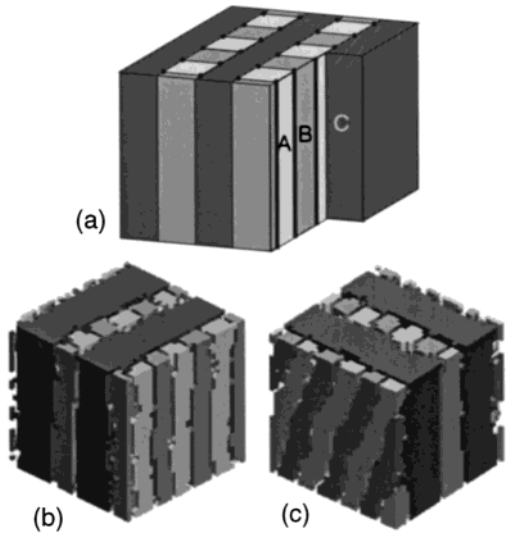

Figure 12. (a) Schematic illustration of the lamella + cylinder (L + C) phase at $3 \le x \le 5$. C arms make lamellar layers and A and B form rectangular cylinders alternately arranged between C layers. JPLs are all straight lines. (b) Snapshot of a simulated structure of $(N_A, N_B, N_C) = (5, 5, 25)$ with $L = 32$. A is light gray, B is medium gray, and C is dark gray. (c) Snapshot of a different simulation run in the same system as part b. The directions of cylinders in different layers are in twisted positions.

The PL has been widely found in the simulations of box sizes $21 \le L \le 43$; this fact is an advantage of the PL structure. We think, however, that it does not immediately mean that the PL is a true stable structure. The reason is as follows. If one quenches this system at a rather high-temperature such as $\beta \approx 0.06$, where A and B components are not sufficiently segregated each other and JPLs do not yet fully develop, the C component shows a strong tendency to make lamellar layers as in the case of diblock copolymers. It would be possible that a similar behavior is seen in the early stage of quenching at $\beta \approx 0.1$. Once C-layers grow, it is difficult for the system to get out of the lamella-like structure at the later stage of quenching.

We must say that none of the above three structures is a decisive one. A conceivable reason we have found several structures is that the region $x \approx 2$ is marginal between the cylindrical and PL phases. For generic microphase-separated structures, there is a recent scenario that bicontinuous phases exist in the boundary region between cylindrical and lamellar phases. Indeed, we have found indications of a new regular network structure in this region, which we must discuss elsewhere.

F. $3 \le x \le 5$: Lamella + Cylinder. For $(N_A, N_B, N_C) = (8, 8, 24)$ and (5, 5, 25), a structure shown in Figure 12 has been found. This is a simple morphology obtained by taking perforation away from the PL structure. We refer to this structure as lamella + cylinder (L + C). Directions of A and B cylinders on both sides of a C-layer can be formed parallel or twisted, as shown in Figure 12, parts b and c. In the twisted case, all JPLs are straight but not parallel, while in the parallel case, the

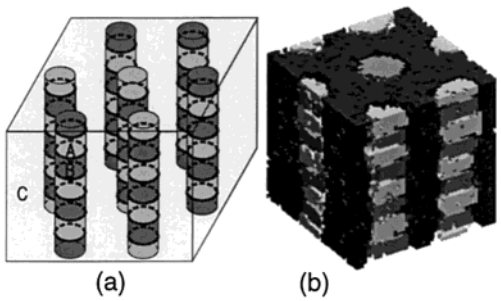

Figure 13. (a) Schematic illustration of the columnar piled disk (CPD) phase obtained at $10 \leq x \leq 15$. In a continuous C matrix, A and B components form disklike domains which are alternately piled and construct a column. All JPLs (thick lines) are circles in this phase. (b) Snapshot of a simulated structure of $(N_A, N_B, N_C) = (5, 5, 50)$ with $L = 38$. A is light gray, B is medium gray, and C is dark gray.

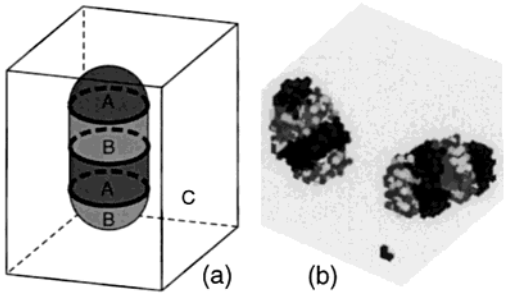

Figure 14. (a) Schematic illustration of the lamella-in-sphere (L-in-S) phase obtained at $x \geq 20$. In a continuous C matrix, A and B components form prolate spherical domains which are composed by alternately piled disks of A and B. All JPLs (thick lines) are circles in this phase. (b) Snapshot of a simulated structure of $(N_A, N_B, N_C) = (4, 4, 80)$ with $L = 26$. A is light gray, B is medium gray, and C is made transparent.

structure is essentially two-dimensional as in the cylindrical structures. There is no topological constraint whether they twist or not; however, mechanical properties such as bending rigidity will be completely different.

G. $6 \leq x \leq 8$: Inverse Perforated Layer. In $x \geq 6$, A and B components together can no longer make layers between C-layers. In almost all simulation runs at $6 \leq x \leq 8$, they form disordered three-dimensional networks which are composed of alternating A and B domains, while the continuous matrix is filled with C components. Since this region is located between lamellar and cylindrical phases, the disordered networks are reminiscent of a complex regular phase as in $x \approx 2$.

As an exception, a perforated layer (or strut structure) composed of alternating A and B components has been observed in the case of $(N_A, N_B, N_C) = (5, 5, 40)$ with $L = 35$. We call it the *inverse perforated layer* (IPL) structure because the roles of AB and C are inverse to the PL structure. However, this structure has not been found in larger simulation boxes, $L \geq 38$. Hence, it is reasonable to consider that the inversely perforated structure has been forced by the boundary conditions of the box. Therefore, we again cannot determine the stable structure in $5 < x < 10$.

H. $10 \leq x \leq 18$: Columnar Piled Disk. Figure 13 shows a structure obtained in $(N_A, N_B, N_C) = (5, 5, 50)$ with $L = 38$. In continuous C-matrix, disklike domains of A and B compose a cylinder by being alternately piled as A−B−A−B−A−. We will call this phase the columnar piled disk (CPD) phase. A−B cylinders seem to be arranged hexagonally. A similar structure has been found in comb-shaped copolymers synthesized by Ruokolainen et al.[17] In the present simulations, the columnar domains consisting of a mixture of A and B have appeared at $\beta = 0.07$ ($N\chi = 77$) and at $\beta \geq 0.15$, where A and B can decompose.

I. $x \geq 20$: Lamella-in-Sphere. When x exceeds 20, the piled-disk columns has been broken apart to form prolate spherical domains at $\beta = 0.06$ ($N\chi \simeq 100$). At this temperature, A and B components did not segregate and the segregation inside spheres occurred at $\beta \geq 0.25$. In many cases, a spherical domain consists of several (typically 4−6) A−B alternating disks as depicted in Figure 14. We call it lamella-in-sphere (L-in-S) phase. This structure is essentially identical with the lamellar-within-spherical phase found in comb-shaped copolymers by Ruokolainen et al.[17] Due to the small size simulation, the numbers of formed spheres in the box were at most 12, and the ordering in the arrangement of the spheres has not been obtained. It is, however, probable that the bcc cubic order or bcc-like order will appear in the real ABC star polymer systems, as in the case of the linear block copolymers.

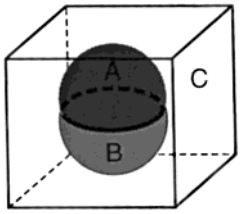

Figure 15. Spherical phase where a sphere is divided into two parts by an equator plane. Contrary to our expectation, this structure has not been obtained in the present study.

We expected the appearance of the structure depicted in Figure 15, which was composed of northern and southern hemispheres. Up to now, it has not been obtained.

IV. Geometry of the Cylindrical Phases

In this section, we present two important properties of the cylindrical phases, which have several kinds of polygons in its sections. First, we present theorem 4.1 that the number of vertices around one polygon must be even. We then discuss the resolution of an experimental case that contradicts with theorem 4.1. Second, on the basis of theorem 4.1, we consider the phases composed of only a single type of JPLs: [8.8.4], [6.6.6], and [12.6.4] are of this type. We call this class the single JPL class. We prove theorem 4.2 that only the three types that have been found can exist. As we have seen in the preceding section, the obtained phases do not always belong to the single JPL class, but physically, it is quite natural to assume that a single physical state is favorable for one star polymers. We presume that the existence of two or more types of JPLs in a phase is due to a few (three!) number of phases belonging to the single JPL class. At the end of this section, some remarks on the phases with plural types of JPLs are given.

A. Even-Polygon Theorem. As stated in section I, we assume that only three interfaces, AB, BC, and CA, exist around one JPL. Then a theorem holds with respect to the cross-section of the cylindrical phase.

Theorem 4.1 (Even-Polygon Theorem): Only Even-Numbered Polygons Appear in the Section of Cylindrical Structures. The proof is obvious from Figure 16. Because of the alternating positions of B and

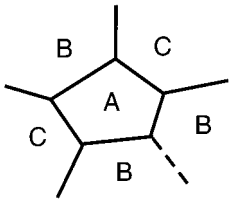

Figure 16. Proof of the even-polygon theorem for cylindrical phases of ABC star polymers: odd-numbered polygons are not allowed because of alternating positions of B and C around an A domain.

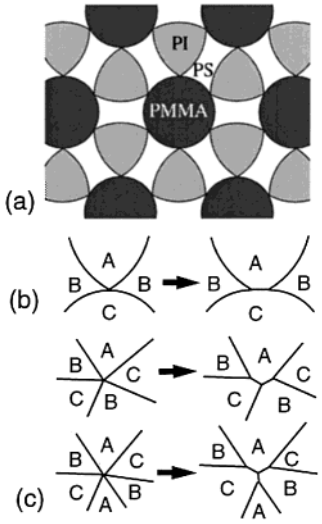

Figure 17. (a) Schematic illustration of the sectional view of a cylindrical phase observed in the star-(PMMA; PI; PS) system by Sioula et al. in ref 27. PMMA and PI have no interface due to strong segregation power between these two components. (b) JPL with four interfaces around itself, that can be interpreted as a couple of JPLs neighboring closely. (c) JPLs with five or more interfaces that can be decomposed similarly.

C around A, odd-numbered polygons are not allowed. This theorem is a strong restriction on the pattern of a cross-section. Actually, the discovered polygons in the present study have been 4-, 6-, 8-, 10-, and 12-gons.

We have assumed that there are always three interfaces around one JPL. However, the possibility of existence of four or more interfaces around a JPL cannot be denied at all. In fact, the case of four interfaces has been reported by Sioula et al.:[27] the sectional view of the case is depicted in Figure 17a. There, PI domains have no interface with PMMA because of strong segregation interactions between PI and PMMA; they are only in contact at the JPL position.

This situation can be solved by interpreting the JPL with four interfaces as a couple of JPLs closely neighboring, as depicted in Figure 17b. Since the segregation power between PI and PMMA is extremely strong, two JPLs might be neighboring within the distance which is comparable to the interface thickness. If the JPL is regarded as two JPLs, the structure becomes equivalent to the [12.6.4] phase. Similarly, a JPL with five or more interfaces can be resolved into two or more JPLs as shown in Figure 17c. Then, the structure should obey the even-polygon theorem.

B. Single JPL Class. Before we present a theorem, which limits the number of allowed cylindrical phases, we take a look at some properties of two-dimensional polygonal tilings. We only assume that a section consists of a single type of JPLs; we relax the condition that N_A is equal to N_B; the areas of A and B polygons in addition to C are not equal. See Figure 18 for the case where N_A is not equal to N_B. Then the lengths of three edges meeting at one vertex are generally not equal. It is obvious that one component can occupy only one type of polygon.

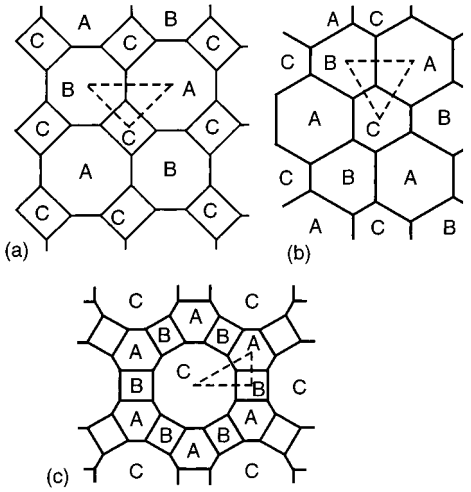

Figure 18. Three cylindrical structures in the single JPL class when all three arm lengths are different, $N_A \neq N_B \neq N_C$, $N_A \neq N_C$: (a) [8.8.4]; (b) [6.6.6]; (c) [12.6.4]. Broken-line triangles connect the centers of the polygons of A, B, and C domains: They are the minimal fundamental triangles that tile the whole plane.

In Figure 18 broken-line triangles are drawn by the perpendicular bisectors of polygon edges. If the triangles are drawn in such a way around all vertices, the triangles are all congruent; the arrangement of JPLs and edges are identical. Then the edge lengths of any polygon should have alternating two values. Each triangle is the minimal fundamental region that can tile the whole plane by mirror symmetric operations. The shape of the minimal fundamental triangle is specific to the phase type and is not dependent on the volume fraction of each component.

When A, B, and C components occupy spaces in k_A-gon, k_B-gon, and k_C-gon, respectively, the number ratio of the polygons in the whole plane is equal to $1/k_A$:$1/k_B$:$1/k_C$, because in the minimal fundamental triangle, there are $1/k_A$, $1/k_B$, and $1/k_C$ fractions of three polygons. Thus, for [8.8.4], [6.6.6], and [12.6.4], the number ratios of polygons in the whole plane are 1:1:2, 1:1:1 and 1:2:3, respectively.

Theorem 4.2: There Are Three and Only Three Types of Tilings for Cylindrical Structures Composed of a Single Type of JPLs. The proof is the following. Since all interior angles at the corner of any polygons are equal, the interior angles of the k-gon must be $(k - 2)\pi/k$ (Figure 18.) If the JPL is referred to as $[k_A, k_B, k_C]$, one obtains by summing up the interior angles around the JPL

$$\frac{k_A - 2}{k_A} + \frac{k_B - 2}{k_B} + \frac{k_C - 2}{k_C} = 2 \qquad (2)$$

Noting k_α is an even-number, we can easily check that possible sets of three numbers $[k_A, k_B, k_C]$satisfying the above equation are only [8.8.4], [6.6.6], and [12.6.4].

This proof is the same as the one in a famous tiling problem called the Archimedean tiling problem.[30] The Archimedean tiling is the tiling by using regular poly-

gons provided that only one type of vertex is permitted. As is distinct from the present problem, four or more polygons can meet at one vertex and odd-numbered polygons are allowed, but polygons are regular in the Archimedean tilings. It is known that only eleven kinds of Archimedean tilings can fill the whole plane.

C. Plural JPL Class. We have seen the strong constraint that the single JPL class contains only three kinds. Here we extend the concept of the JPL class to the plural class: our simulation results [8.6.4; 8.6.6] and [10.6.4; 10.6.4; 10.6.6] are of this type. We call this class the plural JPL type. In this class, prototype polygons are not regular polygons. Under such a condition, mathematically, there may be a countless number of tiling structures.

Nevertheless, if star polymers are monodisperse, it is dubious that there exist a large number of phases in this class, in which star polymers accordingly exhibit complicated physical situations, namely, having a number of different polygons and JPL types. We presume that this physical reasoning restricts possible structures.

As we have seen the above two cases, polygons cannot be regular. However, in simulations, a C component polygon tends to become more like a circular shape, meaning more like a regular polygonal shape, rather than an elongated or irregular polygonal shape. This fact implies that there is a tendency to make the C star arms in the same physical state.

Furthermore, we have counted number densities of junction points per JPL length of two types of JPLs for [8.6.4; 8.6.6] and of three types of JPLs for [10.6.4; 10.6.4; 10.6.6], and we have found no significant difference beyond statistical errors for both phases. Again this fact implies that there is a tendency to make star polymers in the same physical state.

If the junction point densities are all equal, it is then deduced that the ratio of the areas of k_A-gon, k_B-gon, and k_C-gon, is equal to k_A:k_B:xk_C. Actually our experimental area ratio of a hexagon to a tetragon was nearly 3/2.

V. Free Energy in the Strong Segregation Limit for the Single JPL Phases

In this section, we present the mean-field expression of the free energy of ABC star polymer systems in the limit of strong segregation. Actual calculation is restricted to [8.4.4], [6.6.6], [12.6.4], and L + C phases which belong to the single JPL class, because they can be geometrically specified without any additional assumptions provided that interface bending is neglected.

The free energy of ABC star polymer systems are assumed to be the sum of an interfacial energy term F_{IF} and a chain elastic term F_{EL}

$$F = F_{IF} + F_{EL} \tag{3}$$

Here we neglect other nondominant terms, e.g. entropy loss of junction point localization, free energy increase in the vicinity of JPLs and so on.

Helfand and Tagami gave an expression for the interfacial energy of a polymer blend[31]

$$F_{IF} = \frac{k_B T b \chi^{1/2}}{\sqrt{6}\, v} S \tag{4}$$

where k_B is the Boltzmann constant, T is the temperature of the system, b is the bond length, v is the volume of a monomer, χ is the interaction parameter between two polymers, and S is the interface area. In the case of ABC star polymers, three types of interfaces exist i.e. AB, BC, and CA. Total interfacial energy is obtained as

$$F_{IF} = \frac{k_B T b}{\sqrt{6}\, v} \sum_{\alpha\beta} \chi_{\alpha\beta}{}^{1/2} S_{\alpha\beta} \tag{5}$$

where $\chi_{\alpha\beta}$ is the interaction parameter between α and β components and $S_{\alpha\beta}$ is the area of $\alpha\beta$ interfaces per unit cell of the structure. Here, we assume b and v values are equal for all components.

For the elastic term, we use the following formula proposed by Semenov for linear block copolymers[4]

$$F_{EL} = \frac{3}{8}\pi^2 \frac{k_B T}{b^2 N^2 v} \sum_{\alpha=A,B,C} \frac{1}{f_\alpha{}^2} \int_{[\alpha]} R^2(\boldsymbol{r}) d\boldsymbol{r} \tag{6}$$

where N is the polymerization index of a whole polymer, f_α is the fraction of α arms, and $R(\boldsymbol{r})$ is the distance between a point $\boldsymbol{r}$ and the nearest JPL. The integration is carried out over the whole volume of the α domain in the unit cell of the structure. A different point from the case of linear block polymers is that $R(\boldsymbol{r})$ should be always measured from a JPL. In the case of the cylindrical phases, therefore, $R(\boldsymbol{r})$ will be the distance from $\boldsymbol{r}$ to the nearest vertex and the calculation is simplified to two-dimensional integrals. We should like to note that the "dead zone" appears near a JPL;[7] hence, the present estimation should be regarded as the first attempt, and a more accurate evaluation is required in future.

We now introduce a length D that represents the size of the unit cell, and dimensionless parameters a_i which determine the detailed geometry of the morphology. Concrete definitions of D and a_i for some structures are given in Appendix A, and we assume that the height of the unit cell, perpendicular to each section, is equal to a unit length. Extracting D dependence from a unit cell volume $V^{[cell]}$, $S_{\alpha\beta}$, and $\int_{[\alpha]} R^2(\boldsymbol{r}) d\boldsymbol{r}$, one can write

$$V^{[cell]} = D^2 q(a_i) \tag{7}$$

$$S_{\alpha\beta} = D l_{\alpha\beta}(a_i) \tag{8}$$

$$\int_{[\alpha]} R^2(\boldsymbol{r}) d\boldsymbol{r} = D^4 I_\alpha(a_i) \tag{9}$$

where $q(a_i)$, $l_{\alpha\beta}(a_i)$ and $I_\alpha(a_i)$ are morphology dependent functions. Using these expressions, the free energy per one star polymer is reexpressed by multiplying eqs 5 and 6 by $N v/V^{[cell]}$

$$F = \frac{k_B T b N}{\sqrt{6}\, q(a_i)} D^{-1} \sum_{\alpha\beta} \chi_{\alpha\beta}{}^{1/2} l_{\alpha\beta}(a_i) + \frac{3}{8}\pi^2 \frac{k_B T D^2}{b^2 N\, q(a_i)} \sum_{\alpha=A,B,C} \frac{I_\alpha(a_i)}{f_\alpha{}^2} \tag{10}$$

The first term of eq 10 decreases with D, and the second increases; D is determined by

$$\partial F/\partial D = 0 \tag{11}$$

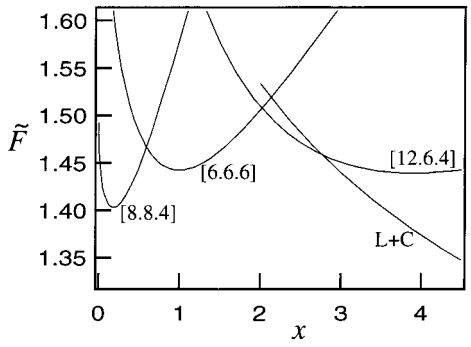

Figure 19. Plot of the reduced free energies $\tilde{F}$ vs x for [8.8.4], [6.6.6], [12.6.4], and L + C phases. With the increase of x, the most stable phase among these four phases varies in order of [8.8.4], [6.6.6], [12.6.4], L + C. The transition points are found to be $x = 0.6$, 2.0, and 2.8, respectively. This behavior agrees with simulation results.

We obtain

$$D = \left[\frac{4\sum_{\alpha\beta}\chi_{\alpha\beta}^{1/2} l_{\alpha\beta}(a_i)}{3\sqrt{6}\pi^2 \sum_{\alpha}\frac{I_\alpha(a_i)}{f_\alpha^2}}\right]^{1/3} N^{2/3} b \tag{12}$$

which yields the minimized free energy $F_{\min}$ as

$$F_{\min} = \frac{3}{4}\pi^{2/3} k_B T N^{1/3} \frac{[\sum_{\alpha\beta}\chi_{\alpha\beta}^{1/2} l_{\alpha\beta}(a_i)]^{2/3}}{q(a_i)} \left[\sum_{\alpha}\frac{I_\alpha(a_i)}{f_\alpha^2}\right]^{1/3} \tag{13}$$

Here D is found to be proportional to $N^{2/3}$, as in the case of linear block copolymers. In the case of symmetric interactions, i.e., $\chi_{AB} = \chi_{BC} = \chi_{CA} = \chi$, eq 13 becomes

$$F_{\min} = \frac{3}{4}\pi^{2/3} k_B T \chi^{1/3} N^{1/3} \frac{l(a_i)^{2/3}}{q(a_i)} \left[\sum_{\alpha}\frac{I_\alpha(a_i)}{f_\alpha^2}\right]^{1/3} \tag{14}$$

Only the last two factors of the right-hand of eq 14 are structure dependent. Thus we evaluate

$$\tilde{F} = \frac{F_{\min}}{\frac{3}{4}\pi^{2/3} k_B T \chi^{1/3} N^{1/3}} \tag{15}$$

Details of the calculation of $\tilde{F}$ are described in Appendix A.

In Figure 19, a plot of the reduced free energy $\tilde{F}$ vs x for [8.8.4], [6.6.6], [12.6.4], and L + C is shown. With the increase of x, the most stable structure varies in the order [8.8.4], [6.6.6], [12.6.4], and L + C; this result is consistent with our simulations. The transition point from [8.8.4] to [6.6.6] is found to be $x = 0.6$ and is slightly smaller than the value $x = 0.7-0.8$ obtained by the simulations. This discrepancy would be improved by taking outward convex boundaries around the C domain in [8.8.4] structure, because it reduces the total interface area in a unit cell, as seen in Appendix B.

As to the [6.6.6] phase, because of the 120° of interface angles, the structure with flat interfaces has the minimal area. Since the sum of the morphology dependent $l_{\alpha\beta}$ of [6.6.6] is independent of x (that is, independent of a, see eq 16). The minimum value of the free energy curve at $x = 1$ in Figure 19 stems from the minimum value of the sum of integrals I_α: When $x = 1$, D is the maximum, the interfacial energy is the minimum, and the elastic term is the minimum.

VI. Conclusion

By using the diagonal bond method (DBM), the morphology of ABC star polymers with arm-length ratio 1:1:x under symmetric interactions was investigated. Our primary goal was to study the fundamental phase behavior with novel morphologies: the phase diagram against x was obtained as Figure 2. We have seen that the DBM is of greatest utility for screening three-dimensional morphologies, while recent publications have been at the level of two-dimensional simulations.[13,15]

As we have summarized the main results in the Introduction, there are two characteristic aspects in the phase behavior shown in Figure 2. One is ordinary phase behavior (points 6−9) in section I known in linear block copolymers, such as lamellae, hexagonal cylinders, and spheres. The other is extraordinary behavior (points 1−5), such as the appearance of JPLs and even-polygonal cylindrical phases.

For the latter, we should like to mention a relationship between star architecture and phase behavior. In ref 12 (see Figure 1 of the paper), in view of space division, we have explained how hetero-arm star architecture strongly influences the geometry of microphase-separated domains for the case of equal arm lengths. According to the paper, ABC star polymers relate to two-dimensional space division. Therefore, in this paper we follow this viewpoint, and we have tried to keep an eye on the issue of geometric constraint concerning JPLs and polygonal tilings. As for the cylindrical phases, the even-polygon theorem and only three, the number of phases in the single JPL class were elucidated, although we have little knowledge of the plural JPL class.

Concerning real polymers, various properties such as polymerization index, dispersion, interaction parameters, persistence length, and glass transition temperatures are different between three components. Therefore, it may be exceptional that two species A and B have such similar properties in this study. ABC star polymers with $N_A \neq N_B$ and/or asymmetric interactions will be addressed in future.

As we have suggested that there may be complex network phases in some regions, we expect that many structures yet remain undiscovered. Our numerical investigation lacks detailed thermodynamic behavior: stability, transition temperatures, scaling properties, and so on. To study the whole story, unfortunately, it is far beyond our computation ability in the state of the art. In addition, the dynamics of ABC star polymer melts, topological defects in new phases, and stepwise transitions are of great interest. Finally, we hope that experimental studies on the morphology of ABC star polymers will be more activated.

Acknowledgment. We are grateful to acknowledge Dr. A. Takano for useful discussions.

Appendix A. Free Energy Calculations

In this appendix, the calculation of $l_{\alpha\beta}$, q and I_α in eq 14 is presented. The cross-sections of [8.8.4], [6.6.6], [12.6.4], and L + C phases are shown in Figures 20a-

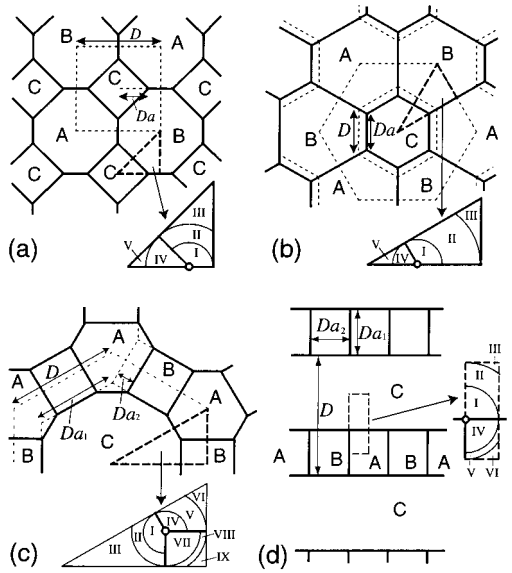

Figure 20. Cross-sections: (a) [8.8.4]; (b) [6.6.6]; (c) [12.6.4]; (d) L + C. *D* represents the size of each unit cell, and lengths a_i are defined in the figures. Magnifications of the dotted-line figures are divided into domains (I, II, ...) of integrals.

20d, where *D* and a_i are defined. The unit cell of each section is designated by broken lines.

$l_{\alpha\beta}(a_i)$ and $q(a_i)$ are obtained from the figures as

$$l_{CA} = l_{BC} = 2\sqrt{2}a$$
$$l_{AB} = 2 - 4a, \quad q = 1 \tag{16}$$

for [8.8.4]

$$l_{CA} = l_{BC} = 3a$$
$$l_{AB} = 9 - 6a, \quad q = \frac{9\sqrt{3}}{2} \tag{17}$$

for [6.6.6]

$$l_{CA} = 6\sqrt{3}a_2, \quad l_{BC} = 6(a_1 - 2a_2)$$
$$l_{AB} = 6\sqrt{3}(1 - a_1), \quad q = \frac{3\sqrt{3}}{2} \tag{18}$$

for [12.6.4], and

$$l_{CA} = l_{BC} = 2a_1a_2$$
$$l_{AB} = 2\,a_1, \quad q = 2\,a_1\,a_2 \tag{19}$$

for L + C.

For the cylindrical phases, the calculation of I_α can be reduced to the two-dimensional integration. Polar coordinates with taking a JPL as the origin are appropriate to evaluate an integral over a region K

$$I_K = \frac{1}{D^4}\int_K R^2(\mathbf{r})d\mathbf{r} \tag{20}$$

where K corresponds to the regions of integration (I, II, ...) which is depicted in the magnifications of dotted line figures of Figure 20.

1. [6.6.6]. The actual calculations of integrals are given as follows

$$I_I = \frac{1}{D^4}\int_0^{Dt_1} dr \int_0^{2\pi/3} d\theta\, r^3 \tag{21}$$

$$I_{II} = \frac{1}{D^4}\int_{Dt_1}^{Dt_2} dr \int_0^{\theta_1} d\theta\, r^3 \tag{22}$$

$$I_{III} = \frac{1}{D^4}\int_{Dt_2}^{Dt_3} dr \int_{\theta_2}^{\theta_1} d\theta\, r^3 \tag{23}$$

$$I_{IV} = \frac{1}{D^4}\int_0^{Da/2} dr \int_0^{\pi/3} d\theta\, r^3 \tag{24}$$

$$I_V = \frac{1}{D^4}\int_{Da/2}^{Da} dr \int_{\theta_3}^{\pi/3} d\theta\, r^3 \tag{25}$$

where

$$t_1 = \frac{a}{2} \tag{26}$$

$$t_2 = \frac{3}{2} - a \tag{27}$$

$$t_3 = \sqrt{a^2 - 3a + 3} \tag{28}$$

$$\theta_1 = \frac{2\pi}{3} - \arccos\left(\frac{Dt_1}{r}\right) \tag{29}$$

$$\theta_2 = \arccos\left(\frac{Dt_2}{r}\right) \tag{30}$$

$$\theta_3 = \arccos\left(\frac{Dt_1}{r}\right) \tag{31}$$

One obtains

$$\frac{1}{6}I_A = \frac{1}{6}I_B = I_I + I_{II} + I_{III} = T\left(\frac{2\pi}{3}, t_1, t_2, t_3\right) \tag{32}$$

and

$$\frac{1}{12}I_C = I_{IV} + I_V = \frac{\sqrt{3}\,a^4}{32} \tag{33}$$

where

$$T(\theta, x, y, z) = \frac{z^4}{4}\theta - \frac{z^4}{4}\arccos\left(\frac{x}{z}\right) - \frac{z^4}{4}\arccos\left(\frac{y}{z}\right) + \frac{y}{12}(2y^2 + z^2)(x\,\mathrm{cosec}\,\theta - y\cot\theta) + \frac{x}{12}(2x^2 + z^2)(y\,\mathrm{cosec}\,\theta - x\cot\theta) \tag{34}$$

$T(\theta, x, y, z)$ corresponds to the sum of integrals for a quadrangular region such as I + II + III in Figure 20b, where θ is an angle at a JPL, *Dx* and *Dy* are lengths of neighboring two edges at both sides of the JPL, and *Dz* is the distance between the JPL and a vertex at the diagonal position of the JPL.

By using the relations

$$f_A = f_B = \frac{1}{2} - \frac{a^2}{6}, \quad f_C = \frac{a^2}{3}, \quad x = \frac{2a^2}{3 - a^2} \tag{35}$$

we can calculate $\tilde{F}$ as a function of *x* for [6.6.6].

2. [8.8.4]. Results for the [8.8.4] phase are similarly obtained as

$$\frac{1}{4}I_A = \frac{1}{4}I_B = I_I + I_{II} + I_{III} = T\left(\frac{3\pi}{4}, t_4, t_5, t_6\right) \quad (36)$$

and

$$\frac{1}{8}I_C = I_{IV} + I_V = \frac{a^4}{12} \quad (37)$$

where

$$t_4 = \frac{1}{2} - a \quad (38)$$

$$t_5 = \frac{a}{\sqrt{2}} \quad (39)$$

$$t_6 = \sqrt{a^2 - a + \frac{1}{2}} \quad (40)$$

Since f_α and x for [8.8.4] are written as

$$f_A = f_B = \frac{1}{2} - a^2, \quad f_C = 2a^2, \quad x = \frac{4a^2}{1 - 2a^2} \quad (41)$$

we can calculate $\tilde{F}$ as a function of x for [8.8.4].

3. [12.6.4]. For [12.6.4], the results of integrations are as follows

$$\frac{1}{12}I_C = I_I + I_{II} + I_{III} = T\left(\frac{5\pi}{6}, t_7, t_8, t_9\right) \quad (42)$$

$$\frac{1}{12}I_A = I_{IV} + I_V + I_{VI} = T\left(\frac{2\pi}{3}, t_7, t_{10}, t_{11}\right) \quad (43)$$

$$\frac{1}{12}I_B = I_{VII} + I_{VIII} + I_{IX} = T\left(\frac{\pi}{2}, t_8, t_{10}, t_{12}\right) \quad (44)$$

where

$$t_7 = \frac{\sqrt{3}}{2}a_2 \quad (45)$$

$$t_8 = \frac{a_1}{2} - a_2 \quad (46)$$

$$t_9 = \sqrt{{a_1}^2 + {a_2}^2 - a_1 a_2} \quad (47)$$

$$t_{10} = \frac{\sqrt{3}\,(1 - a_1)}{2} \quad (48)$$

$$t_{11} = \sqrt{(1 - a_1)^2 + {a_2}^2 + (1 - a_1)a_2} \quad (49)$$

$$t_{12} = \sqrt{{t_8}^2 + {t_{10}}^2} \quad (50)$$

The fractions f_α and the length ratio x for [12.6.4] are

$$f_A = (1 - a_1)^2 + 4\,(1 - a_1)a_2 + {a_2}^2$$

$$f_B = 2\,(1 - a_1)(a_1 - 2a_2)$$

$$f_C = {a_1}^2 - {a_2}^2$$

$$x = \frac{2\,({a_1}^2 - {a_2}^2)}{1 - {a_1}^2 + {a_2}^2} \quad (51)$$

In the case of [12.6.4], the following relation

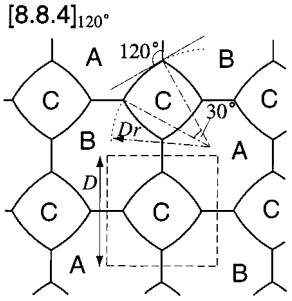

Figure 21. Bend structure of the [8.8.4] cylindrical phase. Interfaces surrounding the C domains are outward convex. The angle between a tangential line at a vertex and an AB interface is 120°. The radius r is determined by eq 63.

$$a_2 = -4\,(1 - a_1) + \sqrt{(1 - a_1)(15 - 13a_1)} \quad (52)$$

is imposed under the condition $f_A = f_B$.

4. L + C. For L + C phase, results are as follows

$$\frac{1}{4}I_C = I_I + I_{II} + I_{III} = T\left(\frac{\pi}{2}, t_{13}, t_{14}, t_{15}\right) \quad (53)$$

$$\frac{1}{2}I_A = \frac{1}{12}I_B = I_{IV} + I_V + I_{VI} = T\left(\frac{\pi}{2}, t_{13}, t_{16}, t_{17}\right) \quad (54)$$

where

$$t_{13} = \frac{a_1 a_2}{2} \quad (55)$$

$$t_{14} = \frac{1 - a_1}{2} \quad (56)$$

$$t_{15} = \sqrt{{t_{13}}^2 + {t_{14}}^2} \quad (57)$$

$$t_{16} = \frac{a_1}{2} \quad (58)$$

$$t_{17} = \sqrt{{t_{13}}^2 + {t_{16}}^2} \quad (59)$$

By using the relations

$$f_A = f_B = \frac{a_1}{2}, \quad f_C = 1 - a_1, \quad x = \frac{2(1 - a_1)}{a_1} \quad (60)$$

we can calculate $\tilde{F}$ as a function of x and a_2. Minimizing the free energy with respect to a_2, then we obtain the final result as a function of x.

Appendix B. Bend Effect of Interfaces in the [8.8.4] Phase

Here, we examine the effect of interface bending on the interfacial energy, taking the [8.8.4] phase as an example. In the straight line approximation of the [8.8.4] structure, three angles between the interfaces around a JPL are 90, 135 and 135°. If all three angles are set to 120° by introducing interface bending,[32] the cross-section will be as shown in Figure 21, where the interfaces surrounding a C domain are drawn by circular arcs with central angle of 30°. Let the radius of this arc be Dr. Then $l_{\alpha\beta}$ and f_C are calculated as

$$l_{AB} = 2 - 2(\sqrt{3} - 1)r \tag{61}$$

$$l_{CA} = l_{BC} = \frac{\pi r}{3} \tag{62}$$

$$f_C = \left(\frac{\pi}{3} - \sqrt{3} + 1\right)r^2 \tag{63}$$

Using the above f_C above, the total interface line length in a unit cell is found to be

$$l_T^{[Bend]} = 2\left[1 + \left(\frac{\pi}{3} - \sqrt{3} + 1\right)^{1/2} f_C^{1/2}\right] \tag{64}$$

On the other hand, the total interface line length of the straight line structure is

$$l_T^{[Straight]} = 2[1 + (2 - \sqrt{2})\, f_C^{1/2}] \tag{65}$$

Because $(\pi/3 - \sqrt{3} + 1)^{1/2} = 0.561$ and $(2 - \sqrt{2}) = 0.586$, the interface area of the bending structure is 0.9% smaller than that of the straight structure at $x = 0.5$.

Note Added after ASAP Posting

This article was released ASAP on 2/22/2002 using the spelling vertexes. This spelling has been changed to vertices. The correct version was posted on 3/7/2002.

References and Notes

(1) Bates, F. S.; Fredrickson, G. H. *Annu. Rev. Phys. Chem.* **1990**, *41*, 525. Bates, F. S.; Fredrickson, G. H. *Phys. Today* **1999**, *52*, No.2, 32.
(2) Hamley, I. W. *The Physics of Block Copolymers*; Oxford University Press: New York, 1998.
(3) Leibler, L. *Macromolecules* **1980**, *13*, 1602.
(4) Semenov, A. N. *Sov. Phys. JETP* **1985**, *61*, 733. Likhtman, A. E.; Semenov, A. N. *Macromolecules* **1994**, *27*, 3103. Phan, S.; Fredrickson, G. H. *Macromolecules* **1998**, *31*, 59.
(5) Ohta, T.; Kawasaki, K. *Macromolecules* **1986**, *19*, 2621. Ohta, T.; Kawasaki, K. *Macromolecules* **1990**, *23*, 2413. Nakazawa, H.; Ohta, T. *Macromolecules* **1993**, *26*, 5503. Nonomura, M.; Ohta, T. *J. Phys. Soc. Jpn.* **2001**, *70*, 927.
(6) Fredrickson, G. H.; Helfand, E. *J. Chem. Phys.* **1987**, *87*, 697.
(7) Milner, S. T.; Witten, T. A.; Cates, M. E. *Macromolecules* **1988**, *21*, 2610.
(8) Matsen, M. W.; Schick, M. *Phys. Rev. Lett.* **1994**, *72*, 2660.
(9) Zheng, W.; Wang, Z.-G. *Macromolecules* **1995**, *28*, 7215.
(10) Dotera, T.; Hatano, A. *J. Chem. Phys.* **1996**, *105*, 8413.
(11) Laladji, M.; Shi, A.-C.; Noolandi, J.; Desai, R. C. *Macromolecules* **1997**, *30*, 3242.
(12) Dotera, T. *Phys. Rev. Lett.* **1999**, *82*, 105.
(13) Drolet, F.; Fredrickson, G. H. *Phys. Rev. Lett.* **1999**, *83*, 4317.
(14) Teramoto, T.; Saeki, A.; Yonezawa, F. *J. Phys. Soc. Jpn.* **2000**, *69*, 679.
(15) Bohbot-Raviv, Y.; Wang, Z.-G. *Phys. Rev. Lett.* **2000**, *85*, 3428.
(16) Hadjichristidis, N. *J. Polym. Sci., Part A* **1999**, *37*, 857.
(17) Ruokolainen, J.; Saariaho, M.; Ikkala, O.; ten Brinke, G.; Thomas, E. L.; Torkkeli, M.; Serimaa, R. *Macromolecules* **1998**, *32*, 1152. Ruokolainen, J.; Makinen, R.; Torkkeli, M.; Makela, T.; Serimaa, R.; ten Brinke, G.; Ikkala, O. *Science* **1998**, *280*, 557. Ruokolainen, J.; ten Brinke, G.; Ikkala, O. *Adv. Mater.* **1999**, *11*, 777.
(18) Saito, R.; Fujita, A.; Ichimura, A.; Ishizu, K. *J. Polym. Sci. A, Polym. Chem. Ed.* **2000**, *38*, 2091.
(19) Fujimoto, T.; Zhang, H.; Kazama, T.; Isono, Y.; Hasegawa, H.; Hashimoto, T. *Polymer* **1992**, *33*, 2208.
(20) Iatrou, H.; Hadjichristidis, N. *Macromolecules* **1992**, *25*, 4649. Hadjichristidis, N.; Iatrou, H.; Behal, S. K.; Chludzinski, J. J.; Disko, M. M.; Garner, R. T.; Liang, K. S.; Lohse, D. J.; Milner, S. T. *Macromolecules* **1993**, *26*, 5812. Floudas, G.; Hadjichristidis, N.; Iatrou, H.; Pakula, T.; W. Fischer, E. *Macromolecules* **1994**, *27*, 7735.
(21) Hückstädt, H.; Abetz, V.; Stadler, R. *Macromol. Rapid Commun.* **1996**, *17*, 599.
(22) Okamoto, O.; Hasegawa, H.; Hashimoto, T.; Fujimoto, T.; Zhang, H.; Kazama, T.; Takano, A.; Isono, Y. *Polymer* **1997**, *38*, 5275.
(23) Sioula, S.; Tselikas, Y.; Hadjichristidis, N. *Macromolecules* **1997**, *30*, 1518. Sioula, S.; Hadjichristidis, N.; Thomas, E. L. *Macromolecules* **1998**, *31*, 5272.
(24) Lambert, O.; Dumas, P.; Hurtrez, G.; Riess, G. *Macromol. Rapid Commun.* **1997**, *18*, 343. Floudas, G.; Reiter, G,; Lambert, O.; Dumas, P. *Macromolecules* **1998**, *31*, 7279.
(25) Lambert, O.; Reutenauer, S.; Hurtrez, G.; Riess, G.; Dumas, P. *Polym. Bull.* **1998**, *40*, 143.
(26) Araki, T.; Takano, A.; Kazama, T.; Isono, Y. *Polym. Prepr., Jpn.* **1998**, *47*, 675. Takano, A.; Sato, S.; Kawahara, S.; Isono, Y. *Polym. Prepr., Jpn.* **1999**, *48*, 2826.
(27) Sioula, S.; Hadjichristidis, N.; Thomas, E. L. *Macromolecules* **1998**, *31*, 8429.
(28) Milner, S. T. *Macromolecules* **1994**, *27*, 2333.
(29) Stadler, R.; Auschra, C.; Beckmann, J.; Krappe, U.; Voigt-Martin, I.; Leibler, L. *Macromolecules* **1995**, *28*, 3080.
(30) Grünbaum, B.; Shephard, G. C. *Tilings and Patterns*; W. H. Freedman and Company: New York, 1986.
(31) Helfand, E.; Tagami, Y. *J. Chem. Phys.* **1971**, *56*, 3592.
(32) Hildebrandt, S.; Tromba, A. *Mathematics and Optimal Form*; W. H. Freeman and Company: New York, 1985.

MA001040Q